

Computational prediction of a +4 oxidation state in Au via compressed AuO₂ compound

Jurong Zhang¹, Xiaolei Feng^{2,3,4,6}, Guangtao Liu^{1,6},
Simon A T Redfern^{3,5} and Hanyu Liu¹

HPSTAR
877-2019

¹ State Key Laboratory for Superhard Materials and Innovation Center of Computational Physics Methods and Software, College of Physics, Jilin University, Changchun 130012, People's Republic of China

² The Institute for Disaster Management and Reconstruction, Sichuan University, Chengdu 61027, People's Republic of China

³ Center for High Pressure Science and Technology Advanced Research (HPSTAR), Shanghai 201203, People's Republic of China

⁴ Department of Earth Sciences, University of Cambridge, Cambridge CB2 3EQ, United Kingdom

⁵ Asian School of the Environment, Nanyang Technological University 639798, Singapore

E-mail: xf232@cam.ac.uk and liuguangtao@jlu.edu.cn

Received 19 July 2019, revised 3 September 2019

Accepted for publication 10 September 2019

Published 14 October 2019



Abstract

Much effort has been devoted to the investigation of the physical and chemical properties of the Au–O system over a range of pressures, owing to the considerable importance of these materials in fundamental and practical applications. To date, however, only Au¹⁺, Au²⁺, Au³⁺, and Au⁵⁺ oxidation states have been identified in the Au–O system, but tetravalent Au⁴⁺ has not been found. Here, we report the results of structure prediction for the Au–O system at high pressure via the effective structure prediction methodology within a first-principles electronic structure framework. We have uncovered an intriguing structure with AuO₂ composition and tetravalent Au, stable at high pressures. This phase shows an electronic transition from a metal to a semiconducting phase as a function of pressure. The present results provide fundamental understanding of the structural and physicochemical properties of compressed Au–O compounds.

Keywords: structure prediction, AuO₂, oxidation states, tetravalent

(Some figures may appear in colour only in the online journal)

Introduction

Gold (Au), being a well-known noble metal, is easily alloyed with other metals, but rarely reacts with other non-metal elements to form compounds [1, 2]. Therefore, much effort has been devoted to exploring the possible existence of unusual valence states for gold. For example, previous theoretical studies have revealed that Au may exhibit valence states ranging from –1 to +6 by combination with elemental lithium or fluorine at high pressures [3, 4]. However, it is well known that lithium and fluorine are extremely difficult to be prepared in high-pressure experiments. In the search

for alternative oxidation states and compounds, the focus has shifted to other potential ligands, including oxygen, which has a high electronegativity value and is relatively easy to handle within the high-pressure experiments.

The most stable structure of gold oxide is Au₂O₃ (*Z* = 8, space symmetry group *Fdd2*) which is found to be stable at ambient conditions [5–7]. Orthorhombic Au₂O₃ contains 40 atoms per cell in the form of a network of AuO₄ units, including two crystallographical distinct types of O atoms and one type of Au atom. This Au₂O₃ compound is a semiconductor with a band gap of about 0.85 eV [5], but it is found to be unstable at high temperature [8]. Au₂O has also been experimentally identified as a breakdown product of Au₂O₃ when it becomes unstable under thermal treatment [8]. High pressure is known

⁶ Authors to whom all correspondence should be addressed.

to be an effective tool to discover new phases with interesting physicochemical properties [9]. A recent high-pressure study [10] reported some new structures of AuO, which contain mixed-valent Au^{1+} and Au^{3+} , as determined from the Bader and projected density of electronic states (PDOS) analysis within PBEsol functional [10]. A similar set of valence states are also reported in a previous study of $\text{Ag}^{1+/3+}\text{O}$ compounds [11]. In a further piece of work [12], a new compound of AuO_2 was identified (space group $C2/m$, $Z = 4$) as stable at 50 GPa, in which Au is mixed-valence $\text{Au}^{3+/5+}$ as computed from the Perdew–Burke–Ernzerhof (PBE) functional. Thus far, the +4 oxidation state of Au has not been found in Au oxides, but only in AuF_4 compounds as predicted under high pressure [3].

Here, we report the results of structure searches for the possible candidates of oxygen-rich compounds in the Au–O system, aiming to identify unusual Au^{4+} . Our results based on the global minimization of free energy surfaces merging *ab initio* total-energy calculations through CALYPSO [13, 14] at high pressure provide useful guidance for further experimental synthesis. We found that a *Pa-3* phase is much more stable than the previously predicted phase [12], indicating Au may have a +4 valence state within the Au–O compounds under pressure. At elevated pressure, it is found that metallic *Pa-3* AuO_2 transforms to a semiconducting *C2/m* phase. According to enthalpy calculations, we propose that the AuO_2 compound with Au^{4+} is expected to form in experiments via the reaction of $\text{Au}_2\text{O}_3 + \text{O}_2$ or $\text{Au} + \text{O}_2$ at high pressure and high temperature.

Computational details

We carried out systematic structure searches of the Au–O system at 0, 25, 50, and 100 GPa via the swarm-intelligence based CALYPSO code, which has been widely and reliably employed in the exploration of a large number of high-pressure systems [15–19]. In structure predictions, each generation contained at least 30 structures, and the first generation was produced randomly with symmetry constraints. The 60% lowest-enthalpy structures from each generation were used to produce the structures in the next generation, using the local particle swarm optimization (PSO) technique, and the remaining 40% of the structures were randomly generated within symmetry constraints to enhance the structural diversity. The CALYPSO method performs global structural minimization of free-energy surfaces combining density functional theory (DFT) calculations with the Vienna *ab initio* simulation package (VASP) [20] code, unbiased by any known structure information. The PBE [21] and PBEsol [22, 23] were adopted for the exchange-correlation functionals. The electron-ion interaction was described using the all-electron projector augmented-wave (PAW) method [24] and $5d^{10}6s^1$ and $2s^22p^4$ were treated as valence electrons for Au and O, respectively. A plane-wave kinetic energy cutoff of 520 eV and dense k -point sampling by Monkhorst–Pack scheme with a grid of 0.025 \AA^{-1} were chosen to ensure that enthalpy calculations converged well. We employed the PHONOPY code [24] to calculate the phonon dispersion curves. Bader’s quantum theory

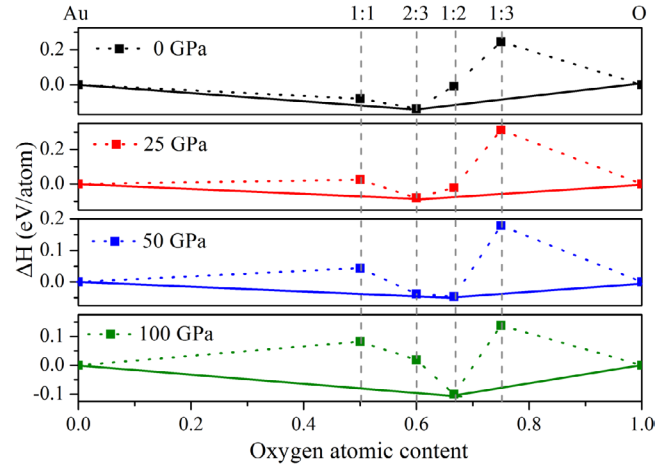


Figure 1. Calculated enthalpy of formation per atom of the Au–O system with respect to decomposition into elemental Au and O. The dashed lines connect the data points, and the solid lines represent the convex hull, where stable phases of O and Au are predicted at different pressures.

Table 1. The lattice constants of Au_2O_3 from the experiment, PBEsol and PBE calculations.

Lattice constants	a (Å)	b (Å)	c (Å)
Experiment [7]	12.827	10.520	3.838
PBEsol	12.860	10.544	3.822
Difference	0.26%	0.2%	0.4%
PBE	13.047	10.696	3.900

[25] of atoms in molecules was used for the analysis of charge populations.

Results and discussion

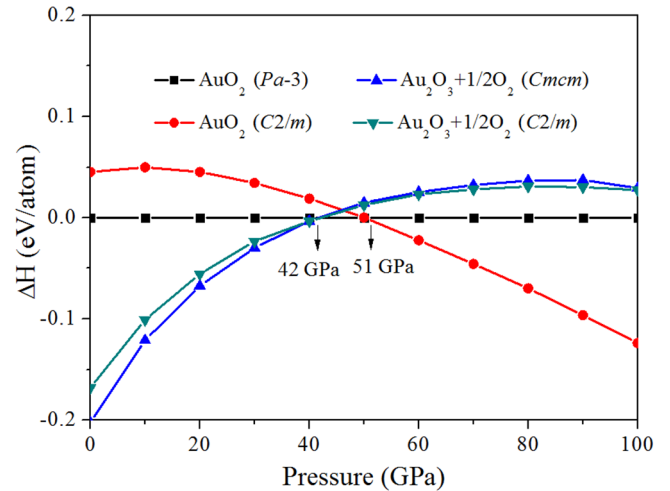
We systematically investigated the chemical stabilities of the Au–O system with 1–4 formula units per unit cell via the formation enthalpies at 0 K, relative to the products of their dissociation into constituent elements (Au and O), as summarized in figure 1. The PBEsol functional is known as a reparameterization of the PBE functional, which is suitable for solids and generally gives better description of experimental lattice constants, elastic properties, and cohesive energies [10, 22, 23]. We thus calculated the lattice constants of Au_2O_3 within PBEsol and PBE functionals at 0 GPa as shown in table 1, where our results are compared with the experimental observations [7]. The differences between the experimental data and PBEsol results for the lattice constants of Au_2O_3 are less than 0.5%, as shown in table 1. It is clearly seen that the PBEsol results are in better agreement with experimental data than the PBE results. The rest of our results are thus calculated within PBEsol functional in this work. Our calculations indicate that *Fdd2* phase of Au_2O_3 is the ground state, in agreement with experimental observations [7], which validates the reliability of our computational scheme. The results indicate that Au_2O_3 gradually becomes unstable as pressure increases, until AuO_2 emerges as the most stable compound, as seen by the fact that it lies on the convex hull shown in figure 1.

Table 2. The lattice parameters and atomic positions of the predicted structures.

Space group	Pressure (GPa)	Parameter	Atomic positions (x, y, z)				
AuO_2 - Pa -3	40	$a = 4.860 \text{ \AA}$	Au1	4a	0.000	0.000	0.000
			O1	8c	0.657	0.657	0.657
	50	$a = 4.822 \text{ \AA}$	Au1	4a	0.000	0.000	0.000
			O1	8c	0.655	0.655	0.655
AuO_2 - $C2/m$	40	$a = 7.667 \text{ \AA}$ $b = 4.476 \text{ \AA}$ $c = 3.468 \text{ \AA}$ $\beta = 68.03^\circ$	Au1	2b	0.500	0.000	0.000
			Au2	2d	0.500	0.000	0.500
			O1	4i	0.799	0.000	-0.095
			O2	4i	0.111	0.000	-0.570
	50	$a = 7.582 \text{ \AA}$ $b = 4.428 \text{ \AA}$ $c = 3.425 \text{ \AA}$ $\beta = 112.03^\circ$	Au1	2b	0.500	0.000	0.000
			Au2	2d	0.500	0.000	0.500
Au_2O_3 - $Fddd$	40	$a = 12.395 \text{ \AA}$ $b = 10.645 \text{ \AA}$ $c = 3.17280 \text{ \AA}$	Au1	16b	-0.452	0.131	-0.186
			O1	16b	-0.917	-0.228	-0.795
			O2	8a	-0.750	-0.250	-0.310
	50	$a = 12.355 \text{ \AA}$ $b = 10.816 \text{ \AA}$ $c = 3.027 \text{ \AA}$	Au1	16b	-0.452	0.131	0.313
			O1	16b	-0.917	-0.226	-0.295
			O2	8a	-0.750	-0.250	0.188

In our structure prediction of the unconventional Au–O compounds, we found two stable phases for AuO_2 with space group Pa -3 and $C2/m$, respectively (table 2). The $C2/m$ phase has been reported previously [12]. We find that the highly symmetric Pa -3 phase of AuO_2 is stable between 42 and 50 GPa (figure 2). The Pa -3 phase takes a lattice constant of $a = 4.822 \text{ \AA}$ (figure 3(a)), which is similar to the pyrite (FeS_2) phase [26]. In this structure, Au and O lie on Wyckoff positions $4a$ (0, 0, 0) and $8c$ (0.656, 0.656, 0.656) at 50 GPa, respectively. In contrast to the Pa -3 phase, in the $C2/m$ phase (figure 3(b)) Au occupies two symmetrically distinct Wyckoff positions Au-I $2b$ (0.5, 0, 0) and Au-II $2d$ (0.5, 0, 0.5), and O also occupies two different Wyckoff positions O-I $4i$ (0.804, 0, -0.08) and O-II $4i$ (0.123, 0, -0.559) at 100 GPa. In the Pa -3 phase of AuO_2 (figure 3(a)), the Au atom is 6-fold coordinated by O to form a distorted AuO_6 octahedron. The Au–O bond length in the Pa -3 phase is 1.971 \AA and the nearest neighbor O–O distance is 2.578 \AA at 50 GPa, suggesting that there is no strong O–O interaction in Pa -3 AuO_2 and AuO_2 is not a peroxide in view of the fact that the covalent radius of O is 0.73 \AA . The Pa -3 structure is composed of octahedral units that share common vertices, where all Au atoms are equivalent. In contrast to the Pa -3 phase, the $C2/m$ phase of AuO_2 is a layer structure, with each layer comprising a plane of AuO_4 groups and AuO_6 octahedra. Two inequivalent Au and O atoms in the $C2/m$ phase (figure 3(b)) form two distinct types of coordination units. One unit consists of one Au atom and four surrounded O atoms; in another Au atom is coordinated by six O atoms, which is similar to the octahedra seen in the Pa -3 phase. In an earlier study of AuO it was reported that the most stable $C2/c$ phase of AuO contains both linear AuO_2 and square-planar AuO_4 groups at 0 GPa, with mixed-valence $\text{Au}^{1+\beta+}$ as reported previously [10].

After investigating the thermodynamic stability of AuO_2 and Au_2O_3 , we checked the dynamical stability by calculating the phonon dispersion relations for these phases using the

**Figure 2.** Ground-state enthalpy curves per formula unit as a function of pressure for AuO_2 (Pa -3 and $C2/m$ phases), with respect to that for the $\text{Au}_2\text{O}_3 + 1/2\text{O}_2$ structure.

finite displacement method as implemented in the Phonopy code [27]. Our calculations confirm that there are no imaginary modes across the entire Brillouin zone, as shown in Fig. 4, demonstrating that these predicted structures are dynamically stable over the pressure range we have considered in this work.

Previous studies have reported the presence of Au^{4+} in AuF_4^3 , however, none were reported in AuO_2^{12} . In the previous work, the suggestion has been made that Au has no single valence state but occurs with mixed +3 and +5 valence states in AuO_2 under pressure. Electronic structures are critical to understanding the related physical and chemical properties of materials [28–30]. As illustrated in our PDOS at 50 and 70 GPa (figure 5), there is strong hybridization between the Au-5d and the O-2p in the valence electrons, indicating that charge is transferred from the Au-5d to O-2p orbitals in our

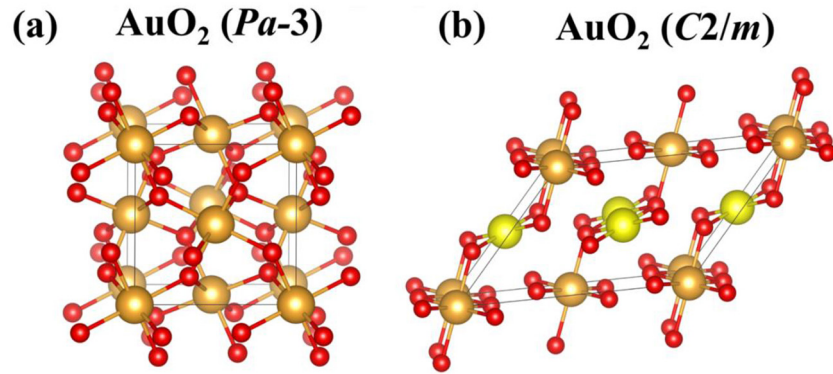


Figure 3. Predicted ground-state and static high-pressure structures for AuO₂: (a) *Pa-3* phase at ambient pressure and (b) *C2/m* phase at 100 GPa.

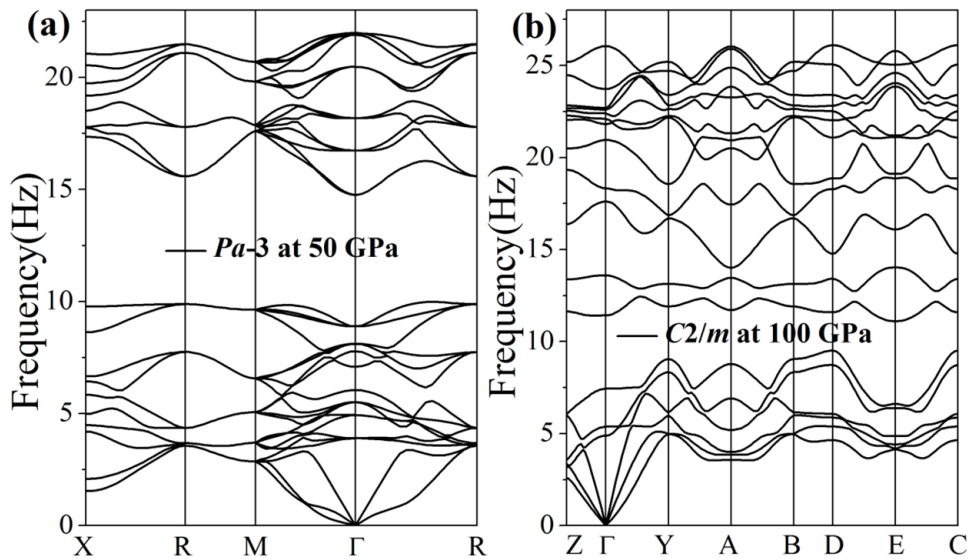


Figure 4. Phonon dispersion curves for the predicted (a) *Pa-3* phase and (b) *C2/m* phase.

AuO₂ compounds. To further illustrate the detailed charge transfer between Au and O atoms, we calculated the Bader charge of the AuO₂ and Au₂O₃ phases with PBEsol functional at 50 GPa. The previous work [7] claimed that Au occurs as Au³⁺ in Au₂O₃, and we found that Au is calculated to lose $\sim 1.32 e$ in our calculations. However, we further found that Au loses $1.63 e$ in our predicted AuO₂ phase (*Pa-3*). Since Au in Au₂O₃ loses $\sim 1.32 e$ and corresponds to a +3 valence state, this suggests that Au in AuO₂ is likely to have +4 valence because $1.63 (\text{AuO}_2)/1.32 (\text{Au}_2^{3+}\text{O}_3)$ is almost equal to $4/3$. We have also performed the Mulliken population analysis [31] that allows to quantitatively provide information about the valence states of Au. In known Au₂O₃ (*Fdd2* phase) with Au³⁺, Au loses $0.89e$; by contrast, Au loses $1.15e$ in AuO₂ (*Pa-3* phase). Their ratio ($1.15/0.89$) is about $4/3$, indicating that the Au in AuO₂ should be Au⁴⁺. Moreover, crystal orbital Hamilton population (COHP) [32] also permits precise analysis of the strength and nature of the chemical bonding for the predicted structure, where ICOHP is the energy integral of COHP and it fundamentally representative chemical interactions between two atoms. The ICOHPs of the AuO₄ unit (in Au₂O₃) and AuO₆ unit (in AuO₂) are -12.52 and -15.84 eV, respectively. The value of $15.84/12.52$ is almost equal to $4/3$, which suggests Au in AuO₂ is +4 valence again.

In this system, both Au₂O₃ and AuO₂ are ionic compounds. We take Au₂O₃ with known Au³⁺ as a good reference to investigate that the valence state of Au is 4+ in AuO₂. Au⁴⁺ is predicted in the Au–O system and it may improve the physical and chemical knowledge of Au. In our calculations, AuO₂ is a pyrite-like structure which has isotropic properties. Some compounds with transition metal having high oxidation state can serve as catalysts, fluorinating agents, and oxidants. Therefore, the newly found AuO₂ is very hopeful to be synthesized experimentally, which may be used as an oxidants like the other useful materials in practical application.

The PDOS and band structures at 50 and 70 GPa for the *Pa-3* phase and *C2/m* phase are added in figures 4(a)–(d). In order to probe the electronic properties of our predicted AuO₂ phase, we calculated the PDOS and electronic band structures. We find that the low-pressure *Pa-3* phase is a metal, as evidenced by the fact that there are occupied states at the Fermi level from the O-*p* orbital to Au-*d* orbital as shown in PDOS. At elevated pressures, its density of state at the Fermi level increases. In contrast, we find that the high-pressure *C2/m* structure is a semiconductor with a gap of 0.32–0.34 eV between 50 and 70 GPa. Band-gap opening may stem from the combined action of orbital hybridization (Au-*d* and O-*p*) and

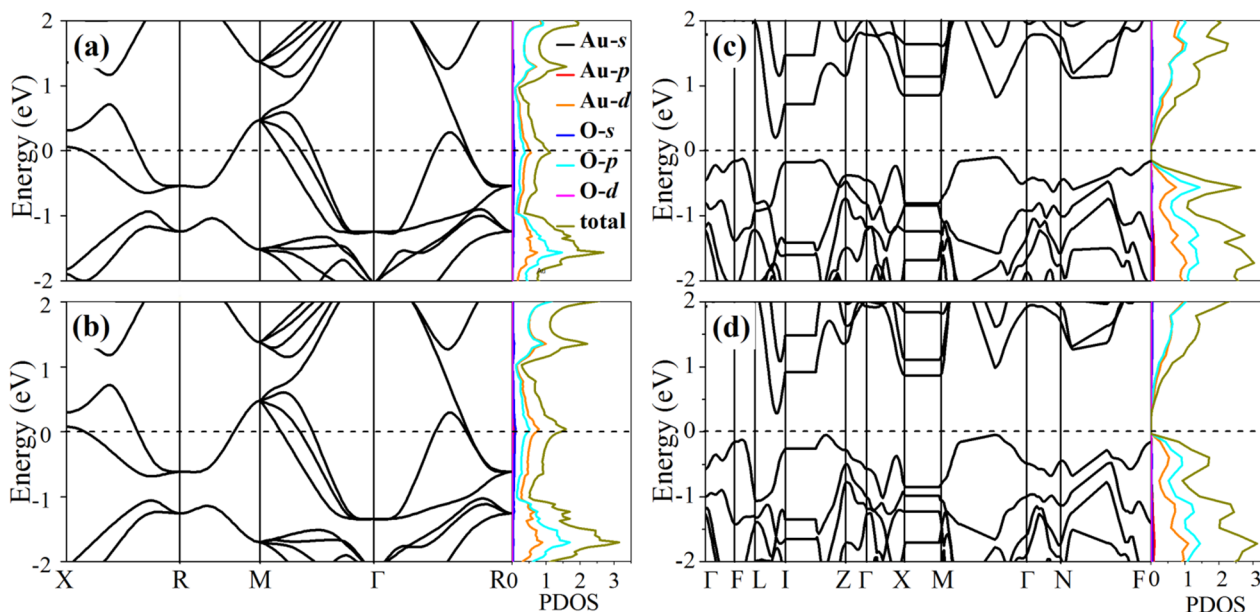


Figure 5. The $Pa-3$ structure (a) and $C2/m$ structure (b) of AuO_2 at 50 and 100 GPa, respectively.

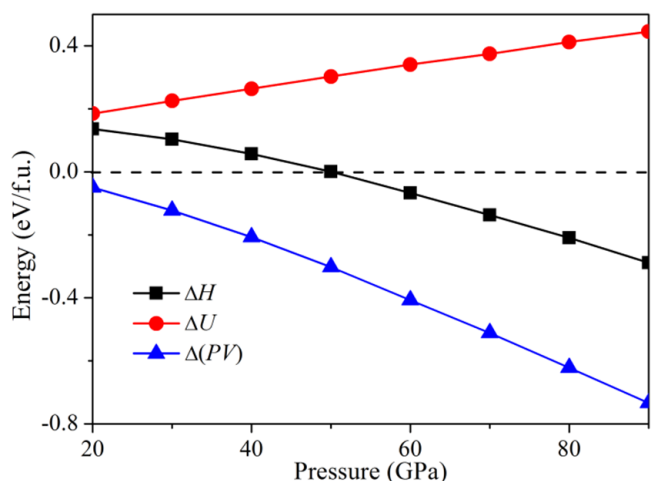


Figure 6. Calculated ΔH , ΔU , and $\Delta(PV)$ versus pressure for the predicted phase transition: from $Pa-3$ phase to $C2/m$ phase. The $Pa-3$ phase is chosen as the reference phase.

the interaction between Au and O, that completely fill the $p-d$ hybridized valence band, similar to the finding in FeH_6 [33].

To further elucidate the mechanisms for the pressure-induced phase transition between the two ionic AuO_2 phases, we examined the evolution of the internal energy (U) and the product of pressure and volume (PV), which contribute to the enthalpy ($H = U + PV$) as a function of pressure. The ΔH , ΔU , and $\Delta(PV)$ are shown in figure 6, where the enthalpy of the $Pa-3$ phase is set to zero. Obviously, the phase transition from $Pa-3$ phase to $C2/m$ phase is mainly caused by the steep decrease of the PV item; meanwhile, the internal energy of the $C2/m$ phase rises with increasing pressure. These results could reasonably explain that $C2/m$ phase could be stable at higher pressure.

Conclusion

In summary, we have identified a new structure of AuO_2 with $Pa-3$ symmetry using the PBEsol functional under high

pressure. We find that the predicted $Pa-3$ phase of AuO_2 contains Au^{4+} , in contrast to the previous finding of mixed-valence states (+3 and +5) in the $C2/m$ phase of AuO_2 . Due to the enhancement of hybridization between Au- d and O- p orbitals, AuO_2 displays an electronic transition from metal to semiconductor upon increasing pressure. Our enthalpy calculations suggest that AuO_2 is much more stable than a mixture of Au_2O_3 and O_2 , indicating that Au-O compounds containing Au^{4+} is hopeful to be synthesized experimentally at high pressure and high temperature from a mixture of Au_2O_3 and O_2 .

Acknowledgments

This work is supported by the National Natural Science Foundation of China (Grants No. 11534003 and 11604314), Science Challenge Project No. TZ2016001, National Science Associated Funding (NSAF, No. U1530124), and the Program for Jilin University Science and Technology Innovative Research Team (JLUSTIRT). We utilized computing facilities at the High-Performance Computing Centre of Jilin University and Tianhe2-JK at the Beijing Computational Science Research Centre. SATR is supported by NERC grant NE/P012167/1. XF is grateful for China Scholarship Council.

ORCID iDs

Jurong Zhang <https://orcid.org/0000-0002-4859-7243>
Guangtao Liu <https://orcid.org/0000-0003-2332-115X>
Simon A T Redfern <https://orcid.org/0000-0001-9513-0147>

References

- [1] Meyer R, Lemire C, Shaikhutdinov S K and Freund H-J 2004 Surface chemistry of catalysis by gold *Gold Bull.* **37** 72–124
- [2] Bond G C and Thompson D T 1999 Catalysis by gold *Catal. Rev.* **41** 319–88

- [3] Lin J, Zhang S, Guan W, Yang G and Ma Y 2018 Gold with +4 and +6 oxidation states in AuF₄ and AuF₆ *J. Am. Chem. Soc.* **140** 9545–50
- [4] Yang G, Wang Y, Peng F, Bergara A and Ma Y 2016 Gold as a 6p-element in dense lithium aurides *J. Am. Chem. Soc.* **138** 4046–52
- [5] Shi H, Asahi R and Stampfl C 2007 Properties of the gold oxides Au₂O₃ and Au₂O: first-principles investigation *Phys. Rev. B* **75** 205125
- [6] Tsai H, Hu E, Perng K, Chen M, Wu J-C and Chang Y-S 2003 Instability of gold oxide Au₂O₃ *Surf. Sci.* **537** L447–50
- [7] Jones P G, Rumpel H, Schwarzmann E, Sheldrick G M and Paulus H 1979 Gold (III) oxide *Acta Crystallogr. B* **35** 1435–7
- [8] Pireaux J, Liehr M, Thiry P, Delrue J and Caudano R 1984 Electron spectroscopic characterization of oxygen adsorption on gold surfaces: II. Production of gold oxide in oxygen DC reactive sputtering *Surf. Sci.* **141** 221–32
- [9] Zhang L, Wang Y, Lv J and Ma Y 2017 Materials discovery at high pressures *Nat. Rev. Mater.* **2** 17005
- [10] Hermann A, Derzsi M, Grochala W and Hoffmann R 2016 AuO: evolving from dis- to comproportionation and back again *Inorg. Chem.* **55** 1278–86
- [11] McMillan J 1960 Magnetic properties and crystalline structure of AgO *J. Inorg. Nucl. Chem.* **13** 28–31
- [12] Tang M, Zhang Y, Li S, Wu X, Jia Y and Yang G 2018 Mixed-valence compounds: AuO₂ and AuS *ChemPhysChem* **19** 2989–94
- [13] Wang Y, Lv J, Zhu L and Ma Y 2010 Crystal structure prediction via particle-swarm optimization *Phys. Rev. B* **82** 094116
- [14] Wang Y, Lv J, Li Q, Wang H and Ma Y 2018 CALYPSO method for structure prediction and its applications to materials discovery *Handbook of Materials Modeling: Applications: Current and Emerging Materials* pp 1–28
- Wang Y, Lv J, Li Q, Wang H and Ma Y 2019 CALYPSO method for structure prediction and its applications to materials discovery *Handbook of Materials Modeling* ed W Andreoni and S Yip (Cham: Springer)
- [15] Liu H, Naumov I I, Hoffmann R, Ashcroft N and Hemley R J 2017 Potential high-*T_c* superconducting lanthanum and yttrium hydrides at high pressure *Proc. Natl Acad. Sci. USA* **114** 6990–5
- [16] Zhu L, Liu H, Pickard C J, Zou G and Ma Y 2014 Reactions of xenon with iron and nickel are predicted in the Earth's inner core *Nat. Chem.* **6** 644
- [17] Feng X, Lu S, Pickard C J, Liu H, Redfern S A and Ma Y 2018 Carbon network evolution from dimers to sheets in superconducting yttrium dicarbide under pressure *Commun. Chem.* **1** 85
- [18] Chen Y, Feng X, Chen J, Cai X, Sun B, Wang H, Du H, Redfern S A, Xie Y and Liu H 2019 Ultrahigh-pressure induced decomposition of silicon disulfide into silicon-sulfur compounds with high coordination numbers *Phys. Rev. B* **99** 184106
- [19] Gao B, Gao P, Lu S, Lv J, Wang Y and Ma Y 2019 Interface structure prediction via CALYPSO method *Sci. Bull.* **64** 301–9
- [20] Kresse G and Furthmüller J 1996 Efficient iterative schemes for *ab initio* total-energy calculations using a plane-wave basis set *Phys. Rev. B* **54** 11169
- [21] Perdew J P, Chevary J A, Vosko S H, Jackson K A, Pederson M R, Singh D J and Fiolhais C 1992 Atoms, molecules, solids, and surfaces: applications of the generalized gradient approximation for exchange and correlation *Phys. Rev. B* **46** 6671
- [22] Haas P, Tran F and Blaha P 2009 Calculation of the lattice constant of solids with semilocal functionals *Phys. Rev. B* **79** 085104
- [23] Csonka G I, Perdew J P, Ruzsinszky A, Philippen P H, Lebègue S, Paier J, Vydrov O A and Ángyán J G 2009 Assessing the performance of recent density functionals for bulk solids *Phys. Rev. B* **79** 155107
- [24] Blöchl P E 1994 Projector augmented-wave method *Phys. Rev. B* **50** 17953
- [25] Bader R F 1985 Atoms in molecules *Acc. Chem. Res.* **18** 9–15
- [26] Brostigen G and Kjekshus A 1969 Redetermined crystal structure of pyrite *Acta Chem. Scand.* **23** 2186–8
- [27] Parlinski K, Li Z and Kawazoe Y 1997 First-principles determination of the soft mode in cubic ZrO₂ *Phys. Rev. Lett.* **78** 4063
- [28] Wang X, Li Y, Pang Y-X, Sun Y, Zhao X-G, Wang J-R and Zhang L 2018 Rational design of new phases of tin monosulfide by first-principles structure searches *Sci. China Phys. Mech. Astron.* **61** 107311
- [29] Sun Y, Wang X, Zhao X-G, Shi Z and Zhang L 2018 First-principle high-throughput calculations of carrier effective masses of two-dimensional transition metal dichalcogenides *J. Semicond.* **39** 072001
- [30] Lu S, Ma W, Jin G, Zeng Q, Feng X, Feng T, Liu H, Meng S, Redfern S A and Yang B 2018 A combined experimental and theoretical investigation of donor and acceptor interface in efficient aqueous-processed polymer/nanocrystal hybrid solar cells *Sci. China Chem.* **61** 437–43
- [31] Mulliken R S 1955 Electronic population analysis on LCAO–MO molecular wave functions. I *J. Chem. Phys.* **23** 1833–40
- [32] Dronskowski R and Blöchl P E 1993 Crystal orbital Hamilton populations (COHP): energy-resolved visualization of chemical bonding in solids based on density-functional calculations *J. Phys. Chem.* **97** 8617–24
- [33] Zhang S, Lin J, Wang Y, Yang G, Bergara A and Ma Y 2018 Nonmetallic FeH₆ under high pressure *J. Chem. Phys.* **122** 12022–8